ACS Infectious Diseases

pubs.acs.org/journal/aidcbc

Article

Investigations into the Antibacterial Mechanism of Action of Viridicatumtoxins

Weijia Li,[#] Li Li,[#] Chao Zhang,[#] Yuanheng Cai,[#] Qiyu Gao, Fulin Wang, Yu Cao, Jinzhong Lin, Jie Li, Zhuo Shang,[*] and Wei Lin[*]

Cite This: *ACS Infect. Dis.* 2020, 6, 1759−1769

Read Online

ACCESS | Metrics & More | Article Recommendations | Supporting Information

ABSTRACT: Viridicatumtoxins are a rare class of tetracycline-like antibiotics that strongly inhibit drug-resistant Gram-positive bacteria. Although reported to exhibit *in vitro* inhibition activity to undecaprenyl pyrophosphate synthase (UPPS), an essential enzyme in bacterial cell wall synthesis, the biological targets and mechanism of action of viridicatumtoxins, especially the drug−target interactions, remain largely unknown. In this study, the structure of *Enterococcus faecalis* UPPS (*Efa*UPPS) was first determined, uncovering that *Efa*UPPS can form not only a typical functional dimer but also an unexpected atypical dimer. We then observed that viridicatumtoxins A (VirA) and B (VirB) are able to bind to UPPSs of *E. faecalis*, *S. aureus*, and *E. coli* in a direct and high-affinity manner as evidenced by *in vitro* enzyme inhibition assay, surface plasmon resonance (SPR) binding analysis, and *in vivo* growth inhibition assay, demonstrating that viridicatumtoxins exert antibacterial effects through UPPS binding. The key amino acid residues involved in the interactions with VirA and VirB in *Efa*UPPS binding pocket were revealed by molecular docking studies, and further validated by site-directed mutagenesis. A single mutation of *Efa*UPPS at D29A, N31A, and R42A can obviously increase their affinities to VirA, while a single mutation at W228A conferred significant resistance to VirA. Moreover, translation inhibition assay showed that VirA and VirB can weakly inhibit *E. coli* 70S ribosome. The weak inhibition of ribosome was proposed to be attributed to steric hindrance between viridicatumtoxin ring F and 70S ribosome helix 34 by molecular docking study. Our structural, biochemical, and computational investigations on the interactions of viridicatumtoxins with UPPS and 70S ribosome not only disclosed the potential biological targets of viridicatumtoxins, but also provided a theoretical basis for structural optimization to make new viridicatumtoxin derivatives with improved antimicrobial activities.

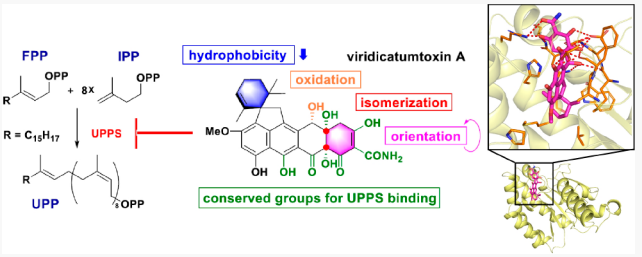

KEYWORDS: *antibiotics, viridicatumtoxins, undecaprenyl pyrophosphate synthase, 70S ribosome, mutagenesis, molecular docking*

The global rise of antimicrobial resistance among bacterial pathogens has rendered most prescribed antibiotics less potent, therefore imposing an urgent need for new antibiotics. In the past century, hundreds of antimicrobial scaffolds have been discovered from nature or designed through chemical synthesis, but only a very small fraction of these chemical entities has been approved for human and veterinary use. The major reason lies in the unsatisfied efficacy, low solubility, improper pharmacokinetics, high toxicity, or easily acquired resistance for most abandoned scaffolds and their derivatives.[1] Understanding the mechanisms of action and the interactions between antimicrobial molecules and their biological targets has opened a venue for antibiotic development, which encourages us to rationally optimize and remodel the abandoned antimicrobial scaffolds for decreased toxicity, improved efficacy, and reduced resistance.

Viridicatumtoxins are an unusual class of antibiotics produced by fungi in the genera *Penicillium* and *Paecilomyces*.[2−7] In addition to a rare geranyl-derived spirobicyclic ring, they possess a naphthacene backbone and substitutions (e.g., carboxamide, phenolic hydroxyl group) that are similar to those of tetracycline antibiotics. Despite high structural similarity, viridicatumtoxins and tetracyclines have different antibacterial spectra. Viridicatumtoxins displayed impressive inhibitory activity against Gram-positive bacteria such as vancomycin-resistant *Enterococci* (VRE) and methicillin-resistant *Staphylococcus aureus* (MRSA) with minimum inhibitory concentrations (MICs) ranging from micromolar to nanomolar, whereas tetracyclines are broad-spectrum antibiotics that are active toward both Gram-positive and -negative pathogens.[8−13] A recent *in vitro* enzyme assay and molecular modeling study suggested that viridicatumtoxin A (VirA) can inhibit *S. aureus* undecaprenyl pyrophosphate

Received: January 19, 2020
Published: May 21, 2020

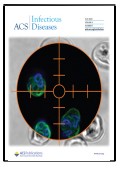

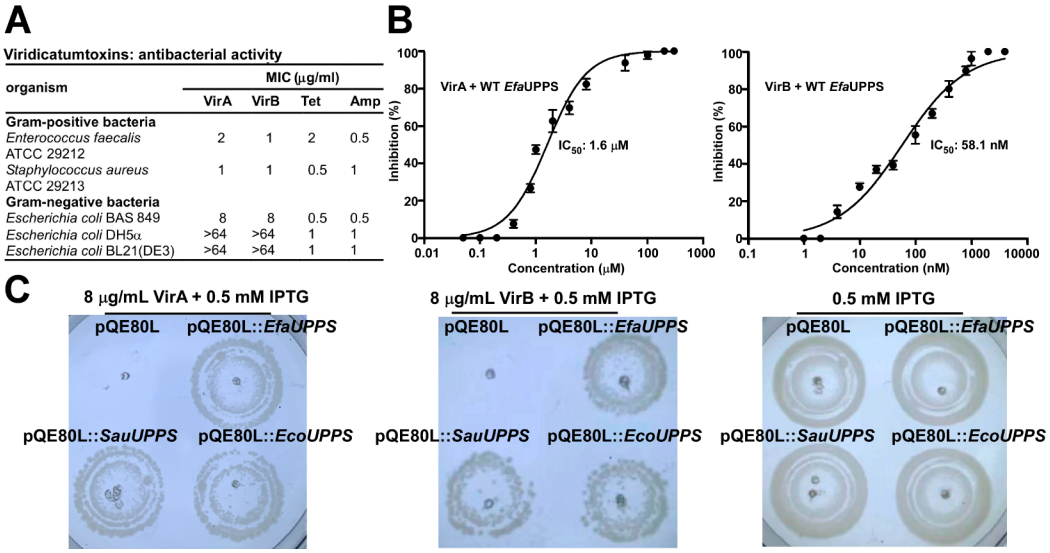

Figure 1. VirA and VirB are strong inhibitors of *Efa*UPPS. (A) Minimum inhibitory concentrations (MICs) of VirA and VirB. Tetracycline (Tet) and ampicillin (Amp) were used as positive controls. (B) *In vitro* inhibitory activities of VirA and VirB toward *Efa*UPPS. The calculated fluorescence percentages were plotted versus antibiotic concentrations on a semilog scale (mean value ± SEM of three biological replicates). (C) *In vivo* growth inhibition assays of VirA (left) and VirB (middle) against *E. coli* BAS 849 transformed with wild-type *Efa*UPPS, *Sau*UPPS, and *Eco*UPPS genes. The strain transformed with the empty vector pQE80L was used as the negative control (right).

synthase (UPPS), an essential cytoplasmic enzyme that catalyzes the formation of undecaprenyl pyrophosphate (UPP or C55-PP) through the consecutive condensation of farnesyl diphosphate (FPP) with eight molecules of isopentenyl diphosphate (IPP). The dephosphorylation of UPP generates undecaprenyl phosphate (UP or C55-P), which serves as a key lipid involved in the biosynthesis of peptidoglycan and a variety of other cell-wall polysaccharide components.[14−20] However, the wrong enantiomer of VirA was used in their molecular modeling study,[18] therefore highly likely resulting in erroneous conclusions. Although UPPS is suggested as a potential biological target of viridicatumtoxins from the *in vitro* enzyme assay, the explicit mechanism of action and the interaction between UPPS and viridicatumtoxins remain uncovered.

In this report, we systematically explored and validated the biological targets of VirA and VirB, two most potent compounds of viridicatumtoxin class, using *in vitro* enzyme inhibition assay, *in vivo* growth inhibition assay, surface plasmon resonance (SPR) binding analysis, and molecular docking studies. Meanwhile, the docked structure of UPPS-viridicatumtoxin complex was computationally simulated based on the crystal structure of *Enterococcus faecalis* UPPS (*Efa*UPPS), and the key amino acid residues in the binding pocket that are involved in the interactions with VirA and VirB were predicted and further validated by site-directed mutation and enzyme kinetics analyses. Our study not only confirmed that viridicatumtoxins exert antibacterial activity through direct binding to UPPS, but also indicated that 70S ribosome might be inhibited by viridicatumtoxins albeit with relatively weak affinity due to possible steric hindrance. The structural information on ligand−enzyme interactions derived from our computational and experimental studies provides a rationale for the optimization and design of new viridicatumtoxin analogues with improved antibiotic activities.

RESULTS AND DISCUSSION

VirA and VirB Are Strong Inhibitors of *Efa*UPPS. To establish an antibacterial dose baseline for viridicatumtoxins, we first tested the antibacterial activities of VirA and VirB by measuring their MICs. As shown in Figure 1A, both VirA and VirB exhibited promising antibacterial effects on *E. faecalis* and *S. aureus* with the MICs ranging from 1 to 2 μg/mL in our broth microdilution assay, which are consistent with previous reports.[6,7] In addition, VirA and VirB also showed moderate inhibitory activities against *Escherichia coli* BAS 849, a strain with deficient outer-membrane structure, with MICs at 8 μg/mL. Previously, Inokoshi et al. performed an enzyme inhibition assay and showed that VirA can inhibit *S. aureus* UPPS activity *in vitro*, suggesting that UPPS is a potential target of viridicatumtoxins.[18]

To validate the proposed target, we first assessed the effects of VirA and VirB on the enzyme activity of the recombinant *E. faecalis* UPPS (*Efa*UPPS) using an enzyme-coupled fluorescence assay. As shown in Figure 1B, both compounds inhibit *Efa*UPPS in a dose-dependent manner with IC_{50} values of 1.6 μM (VirA) and 58.1 nM (VirB), demonstrating that viridicatumtoxins act as strong inhibitors of *Efa*UPPS. Analogously, VirA also displayed strong inhibitory effects on the recombinant *S. aureus* UPPS (*Sau*UPPS) and *E. coli* UPPS (*Eco*UPPS) with comparable IC_{50} values of 4.1 and 3.9 μM, respectively (Figure S1). In contrast, tetracycline (Tet) exhibited moderate inhibitory activity on *Efa*UPPS, *Sau*UPPS, and *Eco*UPPS, the IC_{50} values of which are 12-, 6-, and 6-fold higher than those for VirA (Figure S2).

To further verify that UPPS may be the potential target of viridicatumtoxins *in vivo*, we tested the inhibitory activities of VirA and VirB against UPPS-overexpressed *E. coli* BAS 849. The *E. coli* cells were transformed with plasmids pQE80L::*EfaUPPS*, pQE80L::*SauUPPS*, and pQE80L::*EcoUPPS*, respectively, together with the empty pQE80L plasmid as the negative control. The respective UPPSs were overexpressed in *E. coli* BAS 849 cells in the presence of IPTG (0.5 mM). The

https://dx.doi.org/10.1021/acsinfecdis.0c00031
ACS Infect. Dis. 2020, 6, 1759−1769

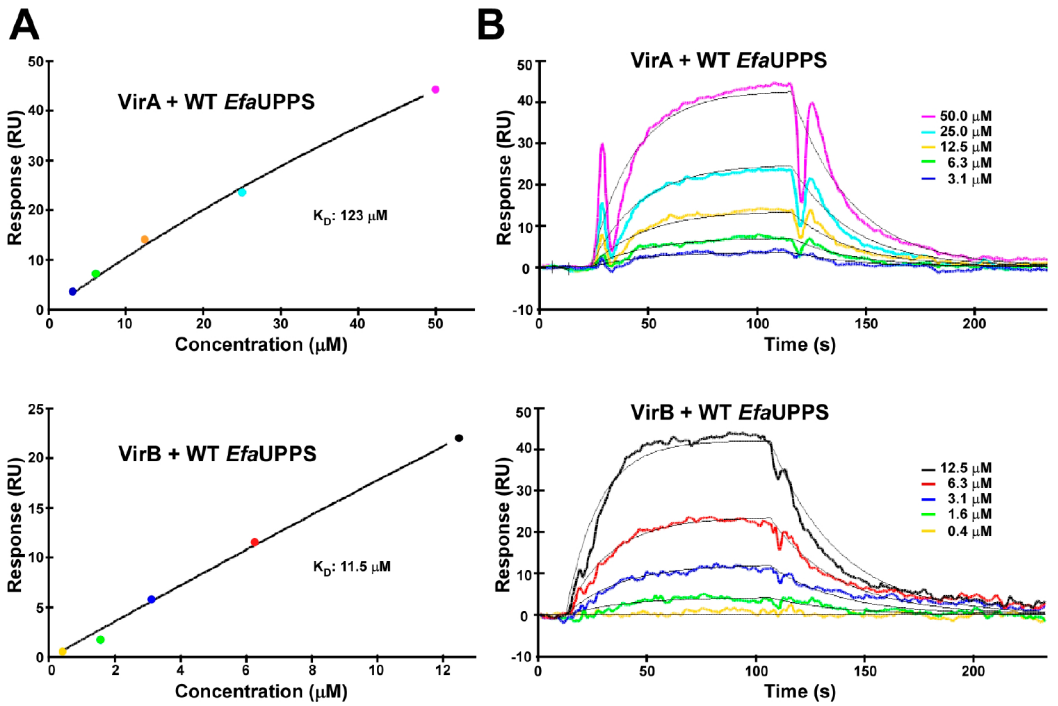

Figure 2. Binding affinities of VirA and VirB to the wild-type *Efa*UPPS measured using surface plasmon resonance (SPR). (A) SPR binding curves for VirA (top) and VirB (bottom) to the wild-type *Efa*UPPS. The dissociation constant (K_D) was shown under each curve. (B) SPR sensorgrams for binding of VirA (top) and VirB (bottom) to the wild-type *Efa*UPPS. The binding affinities of VirA and VirB are in the micromolar range.

results showed that the growth of *E. coli* BAS 849 transformed with the empty vector is completely inhibited by VirA and VirB at 8 μg/mL, but the overexpression of *Efa*UPPS, *Sau*UPPS, and *Eco*UPPS antagonized the antibacterial effect and rescued the cell growth, conferring resistance on the cells (Figure 1C). Interestingly, viridicatumtoxins were previously reported to show inhibitory activities against Gram-positive bacteria exclusively,[6,7] but our studies here revealed that the overexpressed *Eco*UPPS indeed protected the host strains from the killing effects of VirA and VirB like *Efa*UPPS and *Sau*UPPS, suggesting that *Eco*UPPS is also a primary target of viridicatumtoxins. VirA and VirB showed no inhibitory effect against normal *E. coli* species (MIC > 64 μg/mL) consistent with previous reports, whereas they moderately inhibited the outer cell membrane-deficient strain *E. coli* BAS 849 (MIC 8 μg/mL) (Figure 1A), indicating that the outer membrane of Gram-negative bacteria is a major permeability barrier for viridicatumtoxins. Collectively, both the enzyme inhibition assay and the growth inhibition experiment demonstrated that viridicatumtoxins inhibit UPPS activity both *in vitro* and *in vivo*, and bacterial UPPS is a potential target of VirA and VirB to mediate antibiotic sensitivity.

We next applied surface plasmon resonance (SPR) analysis to gain knowledge about whether and how VirA and VirB directly interact with *Efa*UPPS. The biochemical parameters of the binding between VirA/VirB and *Efa*UPPS were measured. Our results showed that the binding mode of VirA/VirB toward *Efa*UPPS could be fit to a one-state binding model, and their equilibrium dissociation constants (K_D) were 123 μM and 11.5 μM, respectively (Figure 2 and Figure S3), suggesting that both VirA and VirB inhibit *Efa*UPPS activity through Mg^{2+}-independent direct binding, and the inhibitory ability of VirB is superior to that of VirA. By contrast, we cannot detect any binding signals between *Efa*UPPS and Tet in our SPR study, although Tet shows moderate inhibition to *Efa*UPPS in *in vitro* enzyme inhibition assay.

Structural Characterization of *Efa*UPPS and Molecular Docking Studies of VirA and VirB. To elucidate the inhibitory mechanism of viridicatumtoxins to UPPS, we purified and crystallized the recombinant *Efa*UPPS from *E. coli* BL21(DE3) cells carrying pET28a-*Efa*UPPS in light of the potent inhibitory activities of VirA and VirB on *E. faecalis*. The crystal data sets were collected and the structure with a resolution of 2.50 Å (PDB ID: 6LOI) for *Efa*UPPS was successfully solved by molecular replacement using the structure of *Eco*UPPS (PDB ID: 1UEH) as a template (*Efa*UPPS shares 58% sequence identity with *Sau*UPPS and 45% sequence identity with *Eco*UPPS, respectively) (Figures S4 and S5). The statistics for data collection and model refinement are listed in Table 1. The overall structure of *Efa*UPPS comprises a central β-sheet with six parallel strands and seven surrounding α-helices (Figure 3A). A flexible loop that is proposed to switch between open (apoenzyme and product-bound) and closed (substrate-bound) conformation has been previously observed in the structure of substrate-bound *Eco*UPPS only, and now is visible in the electron density map of apo *Efa*UPPS (Figure 3A).[21−24]

As shown in Figure 3 and Figure S4, one asymmetric unit consists of six monomers, with two homodimer forms present. Homodimer form I is similar to the functional homodimer as in *Eco*UPPS, where homodimerization occurred through an interface consisting of hydrophobic residues (Figure S4A,B), whereas form II is an atypical homodimer, with its homodimerization interface consisting of hydrophobic and hydrophilic residues (Figure S4C). Two R129 residues in *Efa*UPPS from α4 of both monomers are found stacking against each other by $\pi-\pi$ interactions. R129 further stabilizes the interface by forming a salt bridge and hydrogen bond networks with D97 and Q133 from both monomers. In

https://dx.doi.org/10.1021/acsinfecdis.0c00031
ACS Infect. Dis. 2020, 6, 1759−1769

Table 1. Structure Data Collection and Refinement Statistics

protein	*Efa*UPPS
PDB code	6LOI
data collection source	SSRF BL17U
data collection	
space group	$P3_1$
cell dimensions	
a, b, c (Å)	82.779,82.779,213.706
α, β, γ (deg)	90.0, 90.0, 120.0
resolution (Å)	35.35−2.50(2.65−2.50)[a]
number of unique reflections	54407
R_{merge}	0.166(0.481)[a]
R_{meas}	0.168(0.539)[a]
R_{pim}	0.060(0.269)[a]
$CC_{1/2}$(highest resolution shell)	0.778
$I/\sigma I$	13.25(1.20)[a]
completeness (%)	96.5(69.0)[a]
refinement	
number of unique reflections	46256
number of test reflections	2043
R_{work}/R_{free}	0.19/0.24(0.24/0.30)[a]
number of atoms	
protein	10917
water	205
r.m.s. deviations	
bond lengths (Å)	0.004
bond angles (deg)	0.647
MolProbity statistics	
clashscore	8.10
rotamer outliers(%)	0
Cβ outliers (%)	0
Ramachandran plot	
favored (%)	96
outliers (%)	0

[a]Highest resolution shell in parentheses.

addition, the hydrophobic residues V100, P101, and I104 from both monomers further strengthen the homodimer interactions (Figure S4D).

We also attempted to cocrystallize *Efa*UPPS with VirA/VirB, or soak VirA/VirB into the apo *Efa*UPPS crystals. However, our trials were unsuccessful probably due to the poor aqueous solubility of VirA/VirB and improper crystal packing. Alternatively, we used an *in silico* molecular docking approach to explore the potential interactions between *Efa*UPPS and VirA/VirB. The docking results (Figure 3B,C) and Lineweaver−Burk plots (Figure S6) showed that VirA and VirB can occupy the binding pocket of farnesyl pyrophosphate (FPP), one substrate of *Efa*UPPS, which has been revealed previously in the crystal structure of *Eco*UPPS in complex with FPP (PDB ID: 1V7U), with an estimated binding energy of −3.16 kcal/mol for VirA and −4.84 kcal/mol for VirB. In the molecular docking model, VirA and VirB are surrounded by hydrophobic residues V53, A72, F73, P92, and W228; hydrophilic residues D29, N31, R42, H46, and S74, and amphipathic residues M28 and M50 (Figure 4A,B). The docking model also suggested that the unique lipophilic spirocyclic terpenoid moiety (ring A) of VirA and VirB interacts with M28, M50, V53, A72, F73, and W228, forming a hydrophobic cleft. Furthermore, hydrogen bonds are highly likely formed between 3-hydroxyl group and D29, between the ketone group of primary amide and R42, and between 11-hydroxyl group and S74 for both VirA and VirB (Figure 4B). Particularly, the 5-ketone group of VirB may interact with N31 through a hydrogen bond, while the 5-hydroxyl group of VirA seems to lack strong interaction with *Efa*UPPS. Overall, these results revealed that the binding pocket of VirA and VirB partially overlaps with that of FPP,[22−24] suggesting that viridicatumtoxins may competitively bind UPPS, thus interfering with the conversion from FPP to UPP.

Validation of Key Binding Pocket Residues of *Efa*UPPS. We next sought to experimentally evaluate and verify the interactions between viridicatumtoxins and *Efa*UPPS that were predicted from the molecular docking study. We generated 12 single mutations on critical amino acid residues in the binding pocket of *Efa*UPPS that were proposed to be involved in the interactions with VirA and VirB, and assessed the effects of mutations on *Efa*UPPS enzymatic activity and binding ability. In line with the docking results, VirA seems to be more inclined to bind M28W and M28A mutants than the wild-type UPPS with $IC_{50\text{-}MT}/IC_{50\text{-}WT}$ values of 0.2 and 0.5, respectively (Figure 5A), which was further supported by the observation of increased binding affinity of VirA to M28W mutant (K_D 9.8 μM) in the SPR binding analysis, about 12-fold higher than the wild-type enzyme (Figure 5B,C). The D29A and R42A mutants also become more susceptible to VirA (Figure 5A), possibly because that the replacement of charged amino acids (i.e., Asp, Arg) with hydrophobic ones (i.e., Ala) facilitates VirA to enter the binding pocket. In contrast, five mutated *Efa*UPPSs (M28E, N31E, N31F, H46W, and W228A) turned out to be less susceptible to VirA compared with the wild-type enzyme, with the $IC_{50\text{-}MT}/IC_{50\text{-}WT}$ values being 123.3, 42.4, 10.7, 4.5, and 6.0, respectively (Figure 5A). Consistently, the binding affinity of VirA to N31E mutant was decreased by approximately 3-fold (K_D 322 μM) (Figure 5B,C). The site-directed mutational analysis validated the active sites of *Efa*UPPS and suggested that further reducing the hydrophobicity of terpene moiety may enhance the interactions between VirA/VirB and UPPS, thus increasing its antibacterial ability. It is notable that the changes in $IC_{50\text{-}MT}/IC_{50\text{-}WT}$ of *Efa*UPPS mutants may be attributed to the changes of binding affinity to FPP, and not or partially relevant to VirA. Considering this possibility, we tried to acquire Michaelis−Menten parameters in order to evaluate the binding kinetics between VirA and different *Efa*UPPS mutants. The results suggested that the *Efa*UPPS mutants D29A, N31A, and R42A with decreased $K_{m\text{-}FPP}$ and decreased IC_{50}, N31E, N31F, and H46W with increased $K_{m\text{-}FPP}$ and increased IC_{50}, and W228A with constant $K_{m\text{-}FPP}$ and increased IC_{50} are highly relevant to VirA binding, while the alteration of $IC_{50\text{-}MT}/IC_{50\text{-}WT}$ of the mutants M28W, M28A, F73S, and S74T with increased $K_{m\text{-}FPP}$ and decreased IC_{50}, and M28E with decreased $K_{m\text{-}FPP}$ and increased IC_{50} values are likely attributed to the changed in binding affinity with FPP rather than VirA (Tables S1 and S2). The conclusion is generally in agreement with the *in vivo* inhibition assay of VirA and VirB against *E. coli* BAS 849 expressing different mutated *Efa*UPPSs (Table S3).

VirA and VirB Are Weak Inhibitors of *E. coli* 70S Ribosome. It is well-known that tetracycline (Tet) antibiotics exert a bacteriostatic effect through reversible binding to bacterial 30S ribosomal subunits, and thus interfere with protein synthesis. Viridicatumtoxins are structurally similar to tetracycline antibiotics, as both possess polycyclic naphthacene carboxamide backbone, which is essential to their antibacterial

https://dx.doi.org/10.1021/acsinfecdis.0c00031
ACS Infect. Dis. 2020, 6, 1759−1769

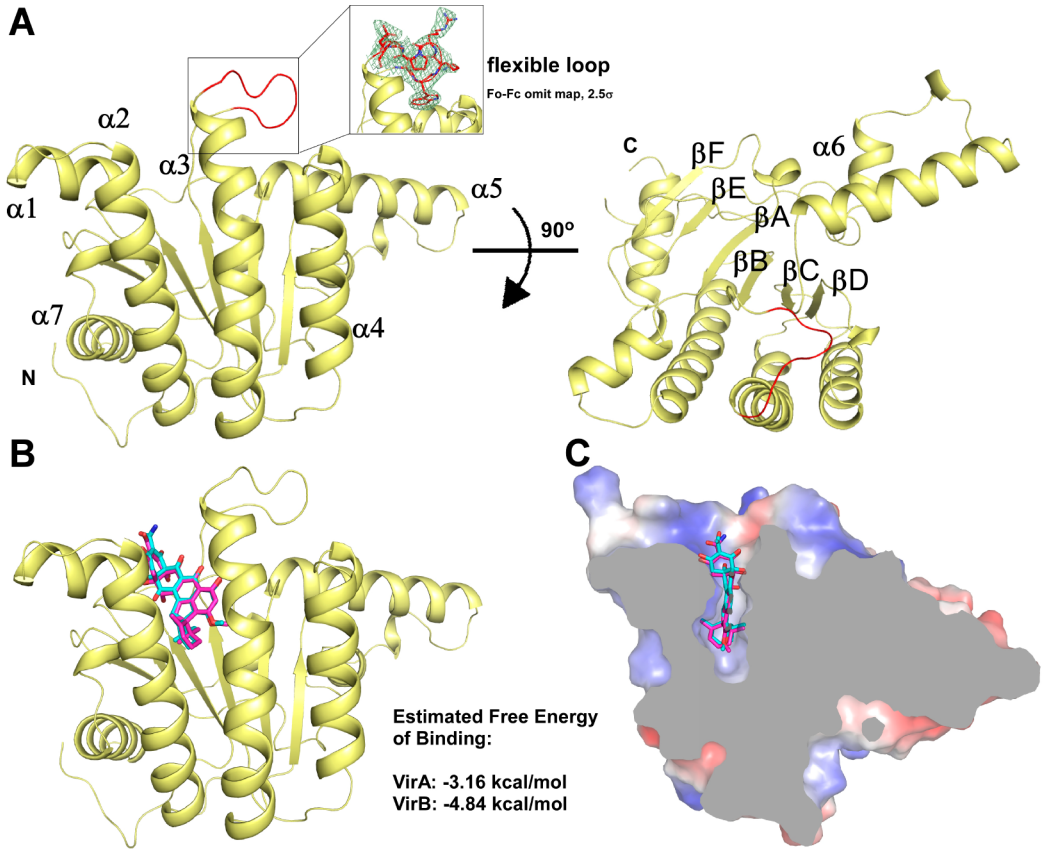

Figure 3. Structure of the wide-type *Efa*UPPS and molecular docking of VirA and VirB with *Efa*UPPS. (A) Overall structure of *Efa*UPPS. *Efa*UPPS is colored in yellow and two orthogonal views are shown. Refined Fo-Fc-omit electron density map (green) contoured at 2.5 σ for the flexible loop (insert figure, top right). (B) Energetically favorable docking models of VirA and VirB to *Efa*UPPS (PDB ID: 6LOI): purple, VirA carbon atoms; cyan, VirB carbon atoms; red, oxygen atoms; blue, nitrogen atoms. (C) Surface electrostatic potential of *Efa*UPPS in complex with VirA and VirB. Colors of compound models are the same as those in part B.

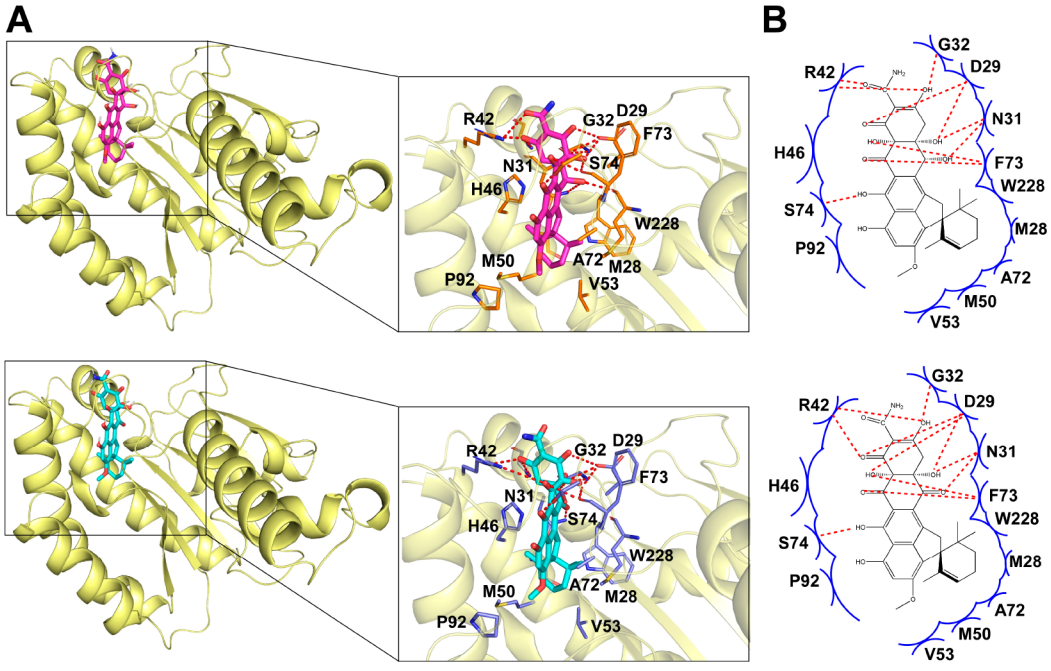

Figure 4. Simulated molecular interactions between VirA/VirB and *Efa*UPPS. (A) Overall structure of *Efa*UPPS enzyme in complex with VirA (purple, top) or VirB (cyan, bottom). The close-up views of simulated VirA/VirB-*Efa*UPPS interactions in the binding pocket are highlighted in black boxes: red stick, oxygen atom; blue stick, nitrogen atom. (B) Summary of the predicted VirA/VirB-*Efa*UPPS interactions where the key amino acid residues involving in the interactions are labeled: red dashed line, hydrogen bond; blue arcs, van der Waals interaction.

https://dx.doi.org/10.1021/acsinfecdis.0c00031
ACS Infect. Dis. 2020, 6, 1759−1769

A Viridicatumtoxins resistance upon substitution at binding site: *Efa*UPPS-inhibitory activity

amino acid substitution	resistance level ($IC_{50\text{-}MT}/IC_{50\text{-}WT}$) VirA
WT	1.0
M28W	0.2
M28A	0.5
M28E	123.3
N31A	0.7
N31E	42.4
N31F	10.7

amino acid substitution	resistance level ($IC_{50\text{-}MT}/IC_{50\text{-}WT}$) VirA
WT	1.0
D29A	0.3
R42A	0.1
H46W	4.5
F73S	0.8
S74T	0.7
W228A	6.0

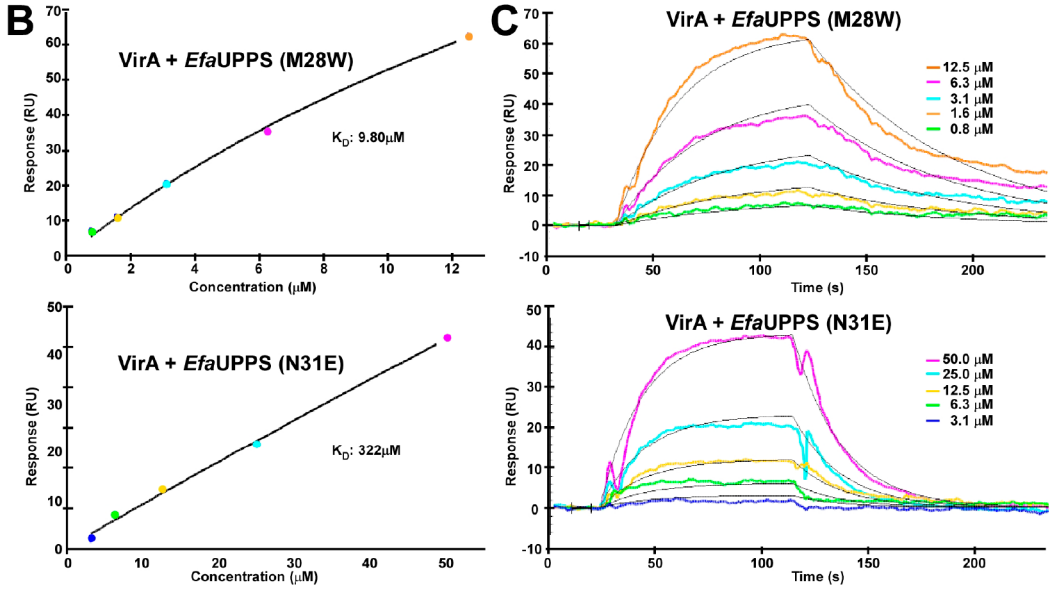

Figure 5. Binding affinity of VirA to the *Efa*UPPS mutants measured by surface plasmon resonance (SPR). (A) Table showing the percentages of *in vitro* inhibitory activities of VirA against different *Efa*UPPS mutants ($IC_{50\text{-}MT}$) compared with the activity of the wild-type *Efa*UPPS ($IC_{50\text{-}WT}$). (B) SPR binding curves for VirA to *Efa*UPPS M28W (top) and N31E (bottom) mutants. The dissociation constant (K_D) was shown under each curve. (C) SPR sensorgrams for binding of VirA to *Efa*UPPS M28W (top) and N31E (bottom) mutants.

ability (Figure 6A). The structural similarity of two classes of antibiotics inspired us to evaluate the inhibitory activity of viridicatumtoxins against bacterial ribosome. Thus, the effects of VirA and VirB on *E. coli* 70S ribosome (composed of 50S and 30S subunits) were assessed using a translation assay that simulates the processes of protein synthesis *in vitro*[9,11] and using an enzyme-coupled fluorescence assay, respectively. The results revealed that both VirA and VirB are able to inhibit *in vitro* translation with a half maximal inhibitory concentration (IC_{50}) of 700 μM and 600 μM in a dose-dependent manner, respectively (Figure 6B). However, compared with tetracycline (Tet) (IC_{50} 15 μM), the inhibitory abilities of VirA and VirB against 70S ribosome are 45-fold lower, inferring that viridicatumtoxins are likely weak inhibitors of *E. coli* 70S ribosome.

Next, we attempted to figure out the possible reasons contributing to the weak interactions between viridicatumtoxins and 70S ribosome using *in silico* molecular modeling and docking. Based on the crystal structure of 70S ribosome−tetracycline complexes of *E. coli* (PDB ID: 5J5B) and *S. aureus* (PDB ID: 5LI0), we generated the modeled structures of 70S ribosome in complex with VirA and VirB, respectively. The energy-optimized docking structures (Figures 6C and S7) clearly revealed that the bottom edges of rings C, D, and E in VirA and VirB are involved in the molecular interaction with Mg^{2+} and bases of 70S ribosome (e.g., C1054, U1196, G1197, and G1198), resembling the binding of tetracycline to 70S ribosome. However, the ring F of VirA and VirB impede such binding to a large extent due to the observed steric hindrance between ring F and helix 34 from 70S ribosome, which may result in the low affinity of viridicatumtoxins to ribosome, while the unique hydrophobic spirocyclic terpene moiety of viridicatumtoxins is not involved in the binding to 70S ribosome. These observations suggested that the affinity of viridicatumtoxins to 70S ribosome could be improved by flipping ring F to the upward direction, therefore eliminating the binding hindrance and enhancing their antibacterial activity. To test this hypothesis, we simulated and docked all four possible VirA isomers whose ring F arrange at different positions [i.e., (4a*S*,12a*S*)-VirA; (4a*R*,12a*S*)-VirA isomer 1; (4a*R*,12a*R*)-VirA isomer 2; (4a*S*,12a*R*)-VirA isomer 3] to 70S ribosome using the same computational program. The generated protein−ligand complex models showed that VirA isomer 1 and VirA isomer 2 (4a*R*,12a*R*) could fit to the binding pocket of 70S ribosome with a relative low free binding energy (−0.11 kcal/mol and −1.43 kcal/mol, respectively), suggesting that simultaneous isomerization of angular hydroxyl groups at C-4a and C-12a of viridicatumtox-

https://dx.doi.org/10.1021/acsinfecdis.0c00031
ACS Infect. Dis. 2020, 6, 1759−1769

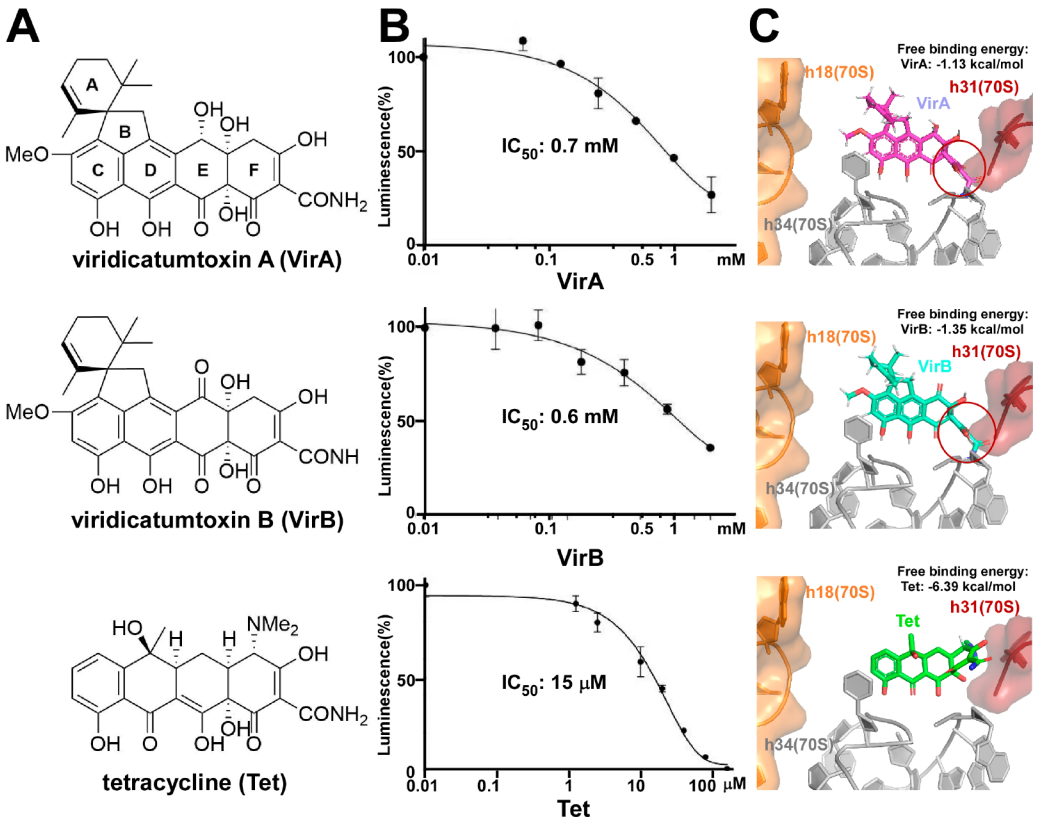

Figure 6. VirA and VirB displayed weak inhibitory activity toward *E. coli* 70S ribosome. (A) Chemical structures of VirA, VirB, and tetracycline (positive control). (B) *In vitro* translation inhibitory activities of VirA, VirB, and tetracycline against *E. coli* 70S ribosome. The calculated luminescence percentages were plotted versus antibiotic concentrations on a semilog scale (mean value ± SEM of three biological replicates). (C) Molecular docking models reveal that the naphthacene backbone of VirA and VirB positions similarly to Tet in the binding pocket of *E. coli* 70S ribosome, while the ring F of VirA (top) and VirB (middle) clashes with ribosome helix 34 as shown in the red cycle. In contrast, the binding pocket of *E. coli* 70S ribosome accommodates Tet according to the crystal structure of ribosome-tetracycline complex (PDB ID: 5J5B). For clarity, the detailed interactions of VirA, VirB, or Tet with *E. coli* 70S ribosome are omitted in the graph.

ins is highly likely to improve their binding affinity to 70S ribosome (Figure S8). However, the isomerization also exerts a significant impact on its binding to *Efa*UPPS. VirA isomer 1 showed an increased binding affinity to *Efa*UPPS (free binding energy −4.58 kcal/mol), but isomer 2 cannot bind to UPPS (Figure S9). This *in silico* prediction provides a rational means for the optimization of viridicatumtoxins to be improved antibiotics and is worthy of being validated by synthetic chemists in the future (Figure S10).

The increasing prevalence of antibiotic resistance has rendered our existing antibiotic arsenal less effective, posing a great threat to modern healthcare worldwide. As the discovery rate of new antibiotic scaffolds has decreased substantially, reinvestigation and redesign of existing scaffolds are becoming alternative ways for new antibiotics. To achieve rational optimization and remodeling of existing antibiotic scaffolds, understanding the biological targets and mechanisms of action as well as drug−target interactions is crucial. These studies will provide a structural basis for high-throughput computational screening of various derivatives and stereoisomers of existing antibiotic scaffolds, from which the structures with higher target-binding affinities are desirable for further chemical modification and synthesis. Herein we reported the biological targets and mechanism of action of viridicatumtoxins, a rare antibiotic class bearing a hybrid terpene-tetracycline scaffold. Our studies confirmed that VirA and VirB strongly inhibit bacterial growth through direct binding to UPPS, a key enzyme in bacterial cell wall synthesis, and may also through weak inhibition of bacterial 70S ribosome translation. The characterization of high-resolution structure of *Efa*UPPS and the determination of *Efa*UPPS key amino acid residues (D29, N31, R42, H46, and W228) involved in the binding of viridicatumtoxins shed light on the drug−enzyme interactions of viridicatumtoxins. This study will inspire the rational optimization of the underexplored viridicatumtoxin scaffold for the purpose of new derivatives with improved antimicrobial activities.

METHODS

Preparation of Viridicatumtoxins A (VirA) and B (VirB). VirA and VirB were prepared according to a previous paper with minor modifications.[6] The marine fungus *Paecilomyces* sp. CMB-F010 was streaked onto PYG agar plates (×120) (2% glucose, 1% peptone, 0.5% yeast extract, and 2% agar, prepared in distilled water) and incubated at 27 °C for 30 days. The resulting agar was sliced into small cubes and extracted with ethyl acetate three times. The ethyl acetate phase was combined and dried under vacuum to yield a crude extract (1.12 g), which was sequentially partitioned with hexane to remove nonpolar components. The hexane-insoluble fraction (785 mg) was further subjected to HPLC chromatography (Phenomenex Luna RP-C_{18}, 250 × 10 mm, 5 μm, 100 Å, 3.5 mL/min isocratic elution with 35% H_2O/MeCN over 20 min, with a constant 0.1% formic acid modifier, monitored at

https://dx.doi.org/10.1021/acsinfecdis.0c00031
ACS Infect. Dis. 2020, 6, 1759−1769

210 and 254 nm) to afford VirA (t_R = 13.5 min, 22.9 mg) and VirB (t_R = 14.9 min, 2.6 mg). The purity (>99%) and structures of VirA and VirB were validated by high performance liquid chromatography (HPLC) coupled with a diode array detector (DAD) and an electrospray LTQ XL linear ion trap mass spectrometer (Thermo Scientific), and a 500 MHz NMR spectrometer (Bruker).

Gene Cloning, Site-Directed Mutagenesis, Expression, and Protein Purification. The undecaprenyl pyrophosphate synthase gene from *Enterococcus faecalis* (*EfaUPPS*) was cloned into the pET28a vector under control of the bacteriophage T7 gene 10 promoter using NdeI and *Hin*dIII. The resulting plasmid was transformed into *E. coli* strain BL21(DE3) (Invitrogen) and selected using 50 μg/mL kanamycin. A single colony of the transformant was used to inoculate 50 mL of LB broth containing 50 μg/mL kanamycin, and the culture was incubated at 200 rpm, 37 °C, for 16 h as a starter culture. An aliquot (10 mL) of the starter culture was then used to inoculate 1 L of LB broth containing 50 μg/mL kanamycin, followed by 37 °C incubation at 200 rpm until reaching an OD_{600} of 0.8. Upon reaching the density, the culture was induced by addition of isopropyl-β-D-thiogalactoside (IPTG) to a final concentration of 1 mM, and shaking at 200 rpm at 16 °C for 16 h. Cells were harvested by centrifugation (4000 × *g*; 15 min at 4 °C), resuspended in buffer A (10 mM Tris-HCl, pH 7.9, 200 mM NaCl, 5 mM DTT, and 5% glycerol), and lysed using an AH-10013 cell disruptor (ATS). The lysate was centrifuged (20,000 × *g*; 30 min at 4 °C), and the cell debris was removed. The supernatant was loaded onto a 5 mL column of Ni-NTA-agarose (Qiagen) pre-equilibrated in buffer A, and the column was washed with 5 mL buffer A (10×) containing 25 mM imidazole and eluted with 50 mL buffer A containing 250 mM imidazole. The eluate was concentrated to ∼10 mg/mL, and further fractionated by gel filtration chromatography on a HiLoad 16/60 Superdex 200 prep grade column (GE Healthcare) in 20 mM Tris-HCl (pH 8.0), containing 100 mM NaCl, 5 mM $MgCl_2$, and 1 mM β-mercaptoethanol. The fraction containing target protein was collected and concentrated to 10 mg/mL in the same buffer using 30 kDa MWCO Amicon Ultra-15 centrifugal ultrafilters (EMD Millipore), and stored in aliquots at −80 °C. The yield of *Efa*UPPS was ∼5 mg/L, and purity was ∼95%. Site-directed mutated *Efa*UPPS derivatives were constructed using site-directed mutagenesis (QuikChange site-directed mutagenesis kit; Agilent) and purified as described for the preparation of wild-type *Efa*UPPS.

Minimal Inhibitory Concentration Assay. The minimal inhibitory concentrations (MICs) of VirA and VirB against *Enterococcus faecalis* ATCC 29212, *Staphylococcus aureus* ATCC 29213, *Escherichia coli* DH5α, *Escherichia coli* BL21-(DE3), *Escherichia coli* BAS 849 (have a defect in outer membrane structure with increased membrane permeability), and *E. coli* BAS 849 mutants transformed with plasmids containing *EfaUPPS* gene with single mutation were determined in Luria−Bertani (LB) broth using the microtiter broth dilution method as described before.[25] Tetracycline (Tet) and ampicillin (Amp) were used as the positive controls. MIC values were means of at least three biological replicates.

***In Vitro* Translation Inhibition Assay.** VirA and VirB were dissolved in DMSO at the concentration of 100 mM. The same concentration of tetracycline was prepared in ethanol as the positive control. A homemade *E. coli in vitro* transcription-translation PURE system was used to assess the inhibitory effects of VirA, VirB, and tetracycline on 70S ribosome activity.[9,11] 5 μL of PURE reaction mix that translates a gene encoding the Nanoluc luciferase was set up in the presence or absence of tested compounds. Protein synthesis was initiated by incubating reactions at 30 °C for 20 min and stopped by placing on ice for 5 min. Luciferase activity was quantified using the Nano-Glo luciferase assay system and read on a GloMax 20/20 luminometer (Promega, USA). For each compound, the *in vitro* translation inhibition assay was performed in three biological triplicates across a series of concentrations from 0.01 to 2 mM. A compound-free control was used to normalize luminescence measurements. The calculated luminescence percentages were plotted versus compound concentrations on a semilog scale using GraphPad Prism (La Jolla, USA).

UPPS Inhibition Assay. The undecaprenyl pyrophosphate synthase (UPPS) reaction was performed in black 96-well microtiter plates (Corning, NY, USA). The purified UPPS enzyme was added to 100 μL of reaction mixture containing 100 mM Tris-HCl (pH 7.5), 0.5 mM $MgCl_2$, 50 mM KCl, 35 μM isopentenyl diphosphate (IPP), 5 μM farnesyl diphosphate (FPP), and 0.005% (*w*/*v*) Triton X-100, with different concentrations of VirA, VirB, or tetracycline (as a negative control). The reaction was carried out at 37 °C, and terminated after 30 min by the addition of 10 μL of 0.5 M EDTA solution. 50 μL of the reaction mixture was transferred into the well of a new 96-well microtiter plate, and quenched with 50 μL of Master Reaction Mix provided in the Pyrophosphate Assay Kit (Sigma-Aldrich, St Louis, USA). After incubating at room temperature for 30 min, the fluorescence of reaction mixture was measured at 316 and 456 nm and read on FlexStation 3 (MD, USA). The calculated fluorescence percentages were plotted versus compound concentrations on a semilog scale using GraphPad Prism (La Jolla, USA). Data of UPPS inhibitory activities were means of at least three biological replicates.

Kinetic Parameters Measurement for Wild-Type *Efa*UPPS and Its Mutants. To measure the kinetic parameters of wild-type *Efa*UPPS and its 12 single-point mutants, 1 μM of each enzyme was used. The reaction was initiated in a 100 μL solution containing 100 mM Tris-HCl (pH 7.5), 0.5 mM $MgCl_2$, 50 mM KCl, 0.005% (*w*/*v*) Triton X-100, and 1 μM of each enzyme tested. For FPP K_m, FPP concentrations were ranged from 0.1 to 20 μM, whereas IPP was 35 μM. The reaction was carried out at 37 °C and terminated by adding 10 μL of 0.5 M EDTA. The product pyrophosphate at each FPP concentration was quantified as stated above. The kinetic parameters (K_m and k_{cat}) were calculated using eq 1.

$$V_0 = V_{max}[S]/(K_m + [S]) \quad (1)$$

where V_0 is the initial velocity, [E] is the enzyme concentration, [S] is the substrate concentration, V_{max} is the maximum velocity, K_m is the Michaelis constant, and k_{cat} is calculated from $V_{max}/[E]$.

For measuring the inhibition constant of VirA to *Efa*UPPS, the procedures and reaction system are similar as the kinetic parameters measurements for *Efa*UPPS shown above except that a series of VirA concentrations (0, 0.5, 1.0, and 5.0 μM final concentration) were added into the reaction system, the kinetic parameters were measured and inhibition constant of VirA was calculated using eq 2.

https://dx.doi.org/10.1021/acsinfecdis.0c00031
ACS Infect. Dis. 2020, 6, 1759−1769

$$1/V_0 = K_m/V_{max}(1 + [I]/K_i)1/[S] + 1/V_{max} \quad (2)$$

In this equation, K_m is the Michaelis constant of the substrate FPP, K_i is the inhibition constant of VirA, V_{max} is the maximal velocity, and [I] and [S] represent the VirA and FPP in the reaction mixture, respectively.

***In Vivo* Growth Inhibition Assay.** The undecaprenyl pyrophosphate synthase genes from *Enterococcus faecalis* ATCC 29212 (*EfaUPPS*), *Staphylococcus aureus* ATCC 29213 (*SauUPPS*), and *Escherichia coli* DH5α (*EcoUPPS*) were cloned into the pQE80L vector under control of the T5 promoter using *Bam*HI and *Hin*dIII. The resulting plasmids were transformed into *E. coli* BAS 849 and selected using 100 μg/mL ampicillin. A single colony of each transformant was inoculated into LB broth supplemented with 100 μg/mL ampicillin and incubated at 200 rpm, 37 °C for 4 h. After diluting the culture to OD_{600} of 0.2 by LB broth, 500 μL of each diluted culture was dripped onto a LB agar plate supplemented with ampicillin (100 μg/mL), IPTG (0.5 mM), and VirA or VirB (8 μg/mL) followed by cultivation at 37 °C overnight. The growth of different *E. coli* BAS 849 transformants in the presence of VirA or VirB was observed.

Surface Plasmon Resonance Binding Assay. Surface plasmon resonance (SPR) analysis was conducted using a Reichert4SPR (Reichert) to evaluate the binding affinity of VirA and VirB to *Efa*UPPS. The standard immobilization protocol (amine coupling method) was used to immobilize *Efa*UPPS (50 μg/mL) on a carboxymethyl dextran chip (Reichert P/N 13206066) to 3758 response units (RU).[26] Different concentrations of VirA and VirB (0.4 μM to 50 μM) were run over SPR with the chip using the running buffer containing 1.8 mM KH_2PO_4, 10 mM Na_2HPO_4, 137 mM NaCl, 2.7 mM KCl, and 0.005% Tween-20, pH 7.8. The binding and dissociation rates were measured at a flow rate of 25 μL/min. The injection of the ligands was done for 1.5 min followed by a flow with ligand-free buffer to analyze the dissociation for 2.5 min. Curves were corrected for nonspecific ligand binding by subtracting the signal obtained for the negative control flow cell. The equilibrium dissociation constant (K_D) was derived from a simple 1:1 interaction model using the Reichert data evaluation software. The SPR sensorgram was obtained by flowing VirA or VirB solution at different concentrations over the *Efa*UPPS immobilized sensor chip, and analyzed using SPR evaluation software. For evaluating the binding affinity of VirA to *Efa*UPPS without Mg^{2+}, The purified *Efa*UPPS was dialyzed twice in a 2 L solution of 25 mM Tris-HCl (pH 7.5), 50 mM KCl, and 1 mM EDTA to remove any Mg^{2+} possibly associated with the enzyme, and then dialyzed twice in a 2 L solution of 25 mM Tris-HCl (pH 7.5) and 50 mM KCl to remove EDTA. After dialysis. The SPR sensorgram was obtained by flowing VirA solution at different concentrations over the *Efa*UPPS without Mg^{2+} immobilized sensor chip, and analyzed using SPR evaluation software.

Crystallization of *Efa*UPPS. Robotic crystallization trials were performed for *Efa*UPPS using a Gryphon liquid handling system (Art Robbins Instruments), commercial screening solutions (Emerald Biosystems, Hampton Research, and Qiagen), and the sitting-drop vapor-diffusion technique (drop: 0.2 μL *Efa*UPPS mixed with 0.2 μL screening solution; reservoir: 60 μL screening solution; 22 °C). 900 conditions were screened in total. Under several conditions, *Efa*UPPS crystals appeared within 1 week. Conditions were optimized using the hanging-drop vapor-diffusion technique at 22 °C. The optimized crystallization condition for *Efa*UPPS was as follows: 0.1 M citrate acid/sodium hydroxide (pH 5.0), 20% (*w*/*v*) PEG 6000 at 22 °C; crystals were transferred into the reservoir solution containing 18% (*v*/*v*) (2*R*,3*R*)-(−)-2,3-butanediol (Sigma-Aldrich) and flash-cooled with liquid nitrogen.

Structure Determination and Refinement of *Efa*UPPS. X-ray diffraction data of *Efa*UPPS were collected from cryo-cooled crystals at SSRL Beamline BL17U (Shanghai Synchrotron Radiation Facility). Data were processed using HKL2000 program.[27] The resolution cutoff criteria were as below: (i) $I/\sigma \geq 1.0$, (ii) $CC_{1/2}$ (highest resolution shell) > 0.5. The structure of *Efa*UPPS was solved by molecular replacement with MOLREP using the structure of UPPS from *E. coli* strain K12 (PDB ID: 1UEH) as a starting model.[28] The molecular replacement solution was outstanding (Top TFZ = 37.7), and an automatic model building was performed using Phenix software package.[21] Additional model building was carried out manually using Coot program and refined by Phenix.[29] The final model of *Efa*UPPS was refined to 2.6 Å resolution with the values of 0.19 (R_{work}) and 0.24 (R_{free}) (Table 1), and deposited in PDB with an accession number of 6LOI.

Molecular Docking Study. All molecular docking studies were performed using Autodock4.2 package.[30] Briefly, chain C of *Efa*UPPS crystal structure was used as the rigid molecule. The molecule was added with nonpolar hydrogens and assigned partial atomic charges using AutoDockTools (ADT).[30] The coordinates of VirB, VirA, and three stereo-isomers were generated using CORINA Classic online service. A grid box with 70 × 90 × 90 grid points and 0.2 Å grid spacing centered roughly at the *Efa*UPPS substrate binding pocket was used as the searching space. 100 runs of Larmarckian Genetic Algorithm were performed to search the protein−ligand interactions. The results were clustered and ranked. Result analyses and figure rendering were performed using PyMOL. To dock VirA and its three stereoisomers to *E. coli* 70S ribosome, the *E. coli* 70S ribosome structure (PDB ID: 5J5B) was used as rigid molecule, and a searching space of 48 × 60 × 60 grid box with 0.2 Å grid spacing around tetracycline binding site was generated. To dock VirA and VirB to *S. aureus* 70S ribosome, the *S. aureus* 70S ribosome structure (PDB ID: 5LI0) was used as rigid molecule and a searching space of 48 × 60 × 60 grid box with 0.1 Å grid spacing around tetracycline binding site was generated. Other parameters were same as *Efa*UPPS docking.

■ ASSOCIATED CONTENT

Supporting Information

The Supporting Information is available free of charge at https://pubs.acs.org/doi/10.1021/acsinfecdis.0c00031.

Crystal structure of *Efa*UPPS, alignment of UPPS genes, and molecular docking studies of VirA isomers(PDF)

PDB structure validation report (PDF)

■ AUTHOR INFORMATION

Corresponding Authors

Zhuo Shang − *Department of Microbiology and Immunology, School of Medicine & Holistic Integrative Medicine, Nanjing University of Chinese Medicine, Nanjing, Jiangsu 210023, China; Department of Chemistry and Biochemistry, University*

https://dx.doi.org/10.1021/acsinfecdis.0c00031
ACS Infect. Dis. 2020, 6, 1759−1769

of South Carolina, Columbia, South Carolina 29208, United States; orcid.org/0000-0002-5755-2629; Email: alexsz1985@gmail.com

Wei Lin − *Department of Microbiology and Immunology, School of Medicine & Holistic Integrative Medicine, Nanjing University of Chinese Medicine, Nanjing, Jiangsu 210023, China; State Key Laboratory of Natural Medicines, China Pharmaceutical University, Nanjing, Jiangsu 211198, China;* orcid.org/0000-0002-2940-6966; Email: weilin@njucm.edu.cn

Authors

Weijia Li − *Department of Microbiology and Immunology, School of Medicine & Holistic Integrative Medicine, Nanjing University of Chinese Medicine, Nanjing, Jiangsu 210023, China*

Li Li − *School of Life Sciences, Fudan University, Shanghai 200433, China*

Chao Zhang − *Department of Pharmacology, School of Medicine & Holistic Integrative Medicine, Nanjing University of Chinese Medicine, Nanjing, Jiangsu 210023, China;* orcid.org/0000-0003-3524-6046

Yuanheng Cai − *Biochemistry and Cell Biology Department, Stony Brook University, Stony Brook, New York 11794, United States*

Qiyu Gao − *Department of Microbiology and Immunology, School of Medicine & Holistic Integrative Medicine, Nanjing University of Chinese Medicine, Nanjing, Jiangsu 210023, China*

Fulin Wang − *Department of Microbiology and Immunology, School of Medicine & Holistic Integrative Medicine, Nanjing University of Chinese Medicine, Nanjing, Jiangsu 210023, China*

Yu Cao − *Department of Microbiology and Immunology, School of Medicine & Holistic Integrative Medicine, Nanjing University of Chinese Medicine, Nanjing, Jiangsu 210023, China*

Jinzhong Lin − *School of Life Sciences, Fudan University, Shanghai 200433, China*

Jie Li − *Department of Chemistry and Biochemistry, University of South Carolina, Columbia, South Carolina 29208, United States*

Complete contact information is available at: https://pubs.acs.org/10.1021/acsinfecdis.0c00031

Author Contributions

#W.L., L.L., C.Z., and Y.C. contributed equally to this work.

Notes

The authors declare no competing financial interest.

■ ACKNOWLEDGMENTS

W.L. acknowledges the financial support in part by National Natural Science Foundation of China (Grant Nos. 81903526 and 81991523), Ying Tung Education Foundation (No. 171033), Natural Science Foundation of Jiangsu Province of China (Grant No. BK20190798), The Open Project of State Key Laboratory of Natural Medicines (No. SKLNMKF202004) and Jiangsu Specially-Appointed Professor Talent Program. Z.S. and J.L. acknowledge a partial financial support by National Institutes of Health (Grant No. P20 GM103641) and National Science Foundation EPSCoR Program (No. OIA-1655740). We thank Prof. Rob Capon (The University of Queensland) for providing the fungus *Paecilomyces* sp. CMB-MF010, and SSRF at Shanghai synchrotron radiation facility for beamline access.

■ ABBREVIATIONS

MRSA, methicillin-resistant *Staphylococcus aureus*; VRE, vancomycin-resistant *Enterococcus*; VirA, viridicatumtoxin A; VirB, viridicatumtoxin B; UPPS, undecaprenyl pyrophosphate synthase; FPP, farnesyl diphosphate; IPP, isopentenyl diphosphate (IPP); *Efa*UPPS, *Enterococcus faecalis* undecaprenyl pyrophosphate synthase; *Sau*UPPS, *Staphylococcus aureus* undecaprenyl pyrophosphate synthase; *Eco*UPPS, *Escherichia coli* undecaprenyl pyrophosphate synthase; SPR, surface plasmon resonance; IPTG, isopropyl β-D-1-thiogalactopyranoside

■ REFERENCES

(1) Kerns, E. H., and Di, L. (2015) *Drug-Like Properties: Concept, Structure Design and Methods, From ADME to Toxicity Optimization*, Academic Press, Elsevier Inc.

(2) Hutchison, R. D., Steyn, P. S., and Van Rensburg, S. J. (1973) Viridicatumtoxin, a new mycotoxin from *Penicillium viridicatum* Westling. *Toxicol. Appl. Pharmacol. 24*, 507−509.

(3) Inokoshi, J., Nakamura, Y., Hongbin, Z., Uchida, R., Nonaka, K., Masuma, R., and Tomoda, H. (2013) Spirohexalines, new inhibitors of bacterial undecaprenyl pyrophosphate synthase, produced by *Penicillium brasilianum* FKI-3368. *J. Antibiot. 66*, 37−41.

(4) Nicolaou, K. C., Hale, C. R., Nilewski, C., Ioannidou, H. A., ElMarrouni, A., Nilewski, L. G., Beabout, K., Wang, T. T., and Shamoo, Y. (2014) Total synthesis of viridicatumtoxin B and analogues thereof: strategy evolution, structural revision, and biological evaluation. *J. Am. Chem. Soc. 136*, 12137−60.

(5) Nicolaou, K. C., Nilewski, C., Hale, C. R., Ioannidou, H. A., ElMarrouni, A., and Koch, L. G. (2013) Total synthesis and structural revision of viridicatumtoxin B. *Angew. Chem., Int. Ed. 52*, 8736−8741.

(6) Shang, Z., Salim, A. A., Khalil, Z., Quezada, M., Bernhardt, P. V., and Capon, R. J. (2015) Viridicatumtoxins: Expanding on a Rare Tetracycline Antibiotic Scaffold. *J. Org. Chem. 80*, 12501−12508.

(7) Zheng, C. J., Yu, H. E., Kim, E. H., and Kim, W. G. (2008) Viridicatumtoxin B, a new anti-MRSA agent from *Penicillium* sp. FR11. *J. Antibiot. 61*, 633−637.

(8) Chopra, I., and Roberts, M. (2001) Tetracycline antibiotics: mode of action, applications, molecular biology, and epidemiology of bacterial resistance. *Microbiol. Mol. Biol. Rev. 65*, 232−260.

(9) Grossman, T. H., Starosta, A. L., Fyfe, C., O'Brien, W., Rothstein, D. M., Mikolajka, A., Wilson, D. N., and Sutcliffe, J. A. (2012) Target- and resistance-based mechanistic studies with TP-434, a novel fluorocycline antibiotic. *Antimicrob. Agents Chemother. 56*, 2559−2564.

(10) Brodersen, D. E., Clemons, W. M., Jr., Carter, A. P., Morgan-Warren, R. J., Wimberly, B. T., and Ramakrishnan, V. (2000) The structural basis for the action of the antibiotics tetracycline, pactamycin, and hygromycin B on the 30S ribosomal subunit. *Cell 103*, 1143−1154.

(11) Jenner, L., Starosta, A. L., Terry, D. S., Mikolajka, A., Filonava, L., Yusupov, M., Blanchard, S. C., Wilson, D. N., and Yusupova, G. (2013) Structural basis for potent inhibitory activity of the antibiotic tigecycline during protein synthesis. *Proc. Natl. Acad. Sci. U. S. A. 110*, 3812−3816.

(12) Olson, M. W., Ruzin, A., Feyfant, E., Rush, T. S., O'Connell, J., and Bradford, P. A. (2006) Functional, biophysical, and structural bases for antibacterial activity of tigecycline. *Antimicrob. Agents Chemother. 50*, 2156−2166.

(13) Schedlbauer, A., Kaminishi, T., Ochoa-Lizarralde, B., Dhimole, N., Zhou, S., Lopez-Alonso, J. P., Connell, S. R., and Fucini, P. (2015) Structural characterization of an alternative mode of tigecycline binding to the bacterial ribosome. *Antimicrob. Agents Chemother. 59*, 2849−2854.

(14) Chang, S. Y., Ko, T. P., Liang, P. H., and Wang, A. H. (2003) Catalytic mechanism revealed by the crystal structure of undecaprenyl pyrophosphate synthase in complex with sulfate, magnesium, and triton. *J. Biol. Chem. 278*, 29298−29307.
(15) Concha, N., Huang, J., Bai, X., Benowitz, A., Brady, P., Grady, L. C., Kryn, L. H., Holmes, D., Ingraham, K., Jin, Q., Pothier Kaushansky, L., McCloskey, L., Messer, J. A., O'Keefe, H., Patel, A., Satz, A. L., Sinnamon, R. H., Schneck, J., Skinner, S. R., Summerfield, J., Taylor, A., Taylor, J. D., Evindar, G., and Stavenger, R. A. (2016) Discovery and characterization of a class of pyrazole inhibitors of bacterial undecaprenyl pyrophosphate synthase. *J. Med. Chem. 59*, 7299−7304.
(16) Czarny, T. L., and Brown, E. D. (2016) A small-molecule screening platform for the discovery of inhibitors of undecaprenyl diphosphate synthase. *ACS Infect. Dis. 2*, 489−499.
(17) Farha, M. A., Czarny, T. L., Myers, C. L., Worrall, L. J., French, S., Conrady, D. G., Wang, Y., Oldfield, E., Strynadka, N. C., and Brown, E. D. (2015) Antagonism screen for inhibitors of bacterial cell wall biogenesis uncovers an inhibitor of undecaprenyl diphosphate synthase. *Proc. Natl. Acad. Sci. U. S. A. 112*, 11048−11053.
(18) Inokoshi, J., Nakamura, Y., Komada, S., Komatsu, K., Umeyama, H., and Tomoda, H. (2016) Inhibition of bacterial undecaprenyl pyrophosphate synthase by small fungal molecules. *J. Antibiot. 69*, 798−805.
(19) Wang, Y., Desai, J., Zhang, Y., Malwal, S. R., Shin, C. J., Feng, X., Sun, H., Liu, G., Guo, R. T., and Oldfield, E. (2016) Bacterial cell growth inhibitors targeting undecaprenyl diphosphate synthase and undecaprenyl diphosphate phosphatase. *ChemMedChem 11*, 2311−2319.
(20) Zhu, W., Zhang, Y., Sinko, W., Hensler, M. E., Olson, J., Molohon, K. J., Lindert, S., Cao, R., Li, K., Wang, K., Wang, Y., Liu, Y. L., Sankovsky, A., de Oliveira, C. A., Mitchell, D. A., Nizet, V., McCammon, J. A., and Oldfield, E. (2013) Antibacterial drug leads targeting isoprenoid biosynthesis. *Proc. Natl. Acad. Sci. U. S. A. 110*, 123−128.
(21) Adams, P. D., Afonine, P. V., Bunkoczi, G., Chen, V. B., Davis, I. W., Echols, N., Headd, J. J., Hung, L. W., Kapral, G. J., Grosse-Kunstleve, R. W., McCoy, A. J., Moriarty, N. W., Oeffner, R., Read, R. J., Richardson, D. C., Richardson, J. S., Terwilliger, T. C., and Zwart, P. H. (2010) PHENIX: a comprehensive Python-based system for macromolecular structure solution. *Acta Crystallogr., Sect. D: Biol. Crystallogr. 66*, 213−221.
(22) El Ghachi, M., Howe, N., Huang, C. Y., Olieric, V., Warshamanage, R., Touze, T., Weichert, D., Stansfeld, P. J., Wang, M., Kerff, F., and Caffrey, M. (2018) Crystal structure of undecaprenyl-pyrophosphate phosphatase and its role in peptidoglycan biosynthesis. *Nat. Commun. 9*, 1078.
(23) Ko, T. P., Huang, C. H., Lai, S. J., and Chen, Y. (2018) Structure of undecaprenyl pyrophosphate synthase from *Acinetobacter baumannii*. *Acta Crystallogr., Sect. F: Struct. Biol. Commun. 74*, 765−769.
(24) Teng, K. H., and Liang, P. H. (2012) Structures, mechanisms and inhibitors of undecaprenyl diphosphate synthase: a *cis*-prenyltransferase for bacterial peptidoglycan biosynthesis. *Bioorg. Chem. 43*, 51−57.
(25) Degen, D., Feng, Y., Zhang, Y., Ebright, K. Y., Ebright, Y. W., Gigliotti, M., Vahedian-Movahed, H., Mandal, S., Talaue, M., Connell, N., Arnold, E., Fenical, W., and Ebright, R. H. (2014) Transcription inhibition by the depsipeptide antibiotic salinamide A. *eLife 3*, e02451.
(26) Lu, C., Kirsch, B., Zimmer, C., de Jong, J. C., Henn, C., Maurer, C. K., Musken, M., Haussler, S., Steinbach, A., and Hartmann, R. W. (2012) Discovery of antagonists of PqsR, a key player in 2-alkyl-4-quinolone-dependent quorum sensing in Pseudomonas aeruginosa. *Chem. Biol. 19*, 381−390.
(27) Otwinowski, Z., and Minor, W. (1997) Processing of X-ray diffraction data collected in oscillation mode. *Methods Enzymol. 276*, 307−326.
(28) Collaborative Computational Project, Number 4 (1994) The CCP4 suite: programs for protein crystallography. *Acta Crystallogr., Sect. D: Biol. Crystallogr. 50*, 760−763.
(29) Emsley, P., Lohkamp, B., Scott, W. G., and Cowtan, K. (2010) Features and development of Coot. *Acta Crystallogr., Sect. D: Biol. Crystallogr. 66*, 486−501.
(30) Morris, G. M., Huey, R., Lindstrom, W., Sanner, M. F., Belew, R. K., Goodsell, D. S., and Olson, A. J. (2009) AutoDock4 and AutoDockTools4: Automated docking with selective receptor flexibility. *J. Comput. Chem. 30*, 2785−2791.

https://dx.doi.org/10.1021/acsinfecdis.0c00031
ACS Infect. Dis. 2020, 6, 1759−1769